Supporting information

Redox engineering of strontium titanate-based thermoelectrics

Andrei V. Kovalevsky* [a], Kiryl V. Zakharchuk [a], Myriam H. Aguirre [b,c], Wenjie Xie [d], Sonia G. Patrício [a], Nuno M. Ferreira [a,e], Diogo Lopes [a], Sergii A. Sergiienko [a], Gabriel Constantinescu [a], Sergey M. Mikhalev [f], Anke Weidenkaff [d], Jorge R. Frade [a]

[a] CICECO – Aveiro Institute of Materials, Department of Materials and Ceramic Engineering, University of Aveiro, 3810-193 Aveiro, Portugal;
[b] Condensed Matter Physics Department, University of Zaragoza and Institute of Material Science of Aragón, ICMA-CSIC, E-50018 Zaragoza, Spain;
[c] Advanced Microscopy Laboratory, I+D Building-Campus Río Ebro, C/Mariano Esquillor s/n, 50018 Zaragoza, Spain;
[d] Materials and Resources, Techn, Universität Darmstadt, Alarich-Weiss Str.2, DE-64287 Darmstadt, Germany;
[e] i3N, Physics Department, University of Aveiro, 3810-193 Aveiro, Portugal
[f] TEMA-NRD, Mechanical Engineering Department, Aveiro Institute of Nanotechnology (AIN), University of Aveiro, 3810-193 Aveiro, Portugal

* Corresponding author. Present address: Department of Materials and Ceramic Engineering, CICECO-Aveiro Institute of Materials, University of Aveiro, 3810-193 Aveiro, Portugal.
Fax: +351-234-370204; Tel: +351-234-370235; E-mail: akavaleuski@ua.pt

Table S1

Binding energies and relative areas of Ti 2p and Mo 3d core-levels for $Sr(Ti,Mo)O_{3\pm\delta}$ ceramics obtained by curve fitting of XPS spectra.

Composition	**Ti 2p 3/2**		**Ti 2p 1/2**		**Mo 3d 5/2**		**Mo 3d 3/2**	
	BE, eV[a]	Area, %[b]	BE, eV[a]	Area, %[b]	BE, eV[a]	Area, %[b]	BE, eV[a]	Area, %[b]
$Sr_{1.00}Ti_{0.94}Mo_{0.06}O_{3\pm\delta}$	457.2 (1.10)	3.0	463.4 (2.00)	1.5	227.8 (0.80)	2.6	230.9 (0.96)	1.8
	458.6 (1.10)	63.3	464.4 (2.00)	32.2	230.5 (1.28)	14.4	233.6 (1.40)	10.0
					231.9 (1.28)	19.4	235.0 (1.40)	13.3
					232.8 (1.28)	22.8	236.0 (1.40)	15.7
$Sr_{0.97}Ti_{0.94}Mo_{0.06}O_{3\pm\delta}$	457.0 (1.13)	2.1	463.1 (2.01)	1.1	227.8 (0.66)	24.2	230.9 (0.86)	16.9
	458.5 (1.13)	64.2	464.3 (2.01)	32.6	230.5 (1.22)	3.6	233.6 (1.44)	2.6
					231.8 (1.22)	11.1	235.0 (1.44)	7.8
					232.8 (1.22)	19.9	235.9 (1.44)	13.9
$Sr_{1.00}Ti_{0.97}Mo_{0.03}O_{3\pm\delta}$	457.2 (1.08)	1.9	463.3 (1.97)	1.0	227.8 (0.50)	2.9	230.9 (0.80)	2.1
	458.6 (1.08)	64.4	464.4 (1.97)	32.7	230.7 (1.17)	11.4	233.8 (1.13)	7.8
					232.1 (1.17)	28.7	235.2 (1.13)	19.7
					233.1 (1.17)	16.2	236.2 (1.13)	11.2

[a]Values between brackets refer to the FWHM (full-width at half maximum) of bands;
[b]Area of each component relative to the total core-level peak area.

Table S2

Relative fractions of titanium and molybdenum oxidation states (in %) calculated from the XPS high resolution spectra.

Composition	$[Ti^{3+}]/[Ti]_{tot}$	$[Mo^{6+}]/[Mo]_{tot}$	$[Mo^{5+}]/[Mo]_{tot}$	$[Mo^{4+}]/[Mo]_{tot}$	$[Mo^{0}]/[Mo]_{tot}$
$SrTi_{0.97}Mo_{0.03}O_3$	2.9	27.4	48.4	19.2	5.0
$SrTi_{0.94}Mo_{0.06}O_3$	4.5	38.6	32.7	24.4	4.3
$Sr_{0.97}Ti_{0.94}Mo_{0.06}O_3$	3.2	33.8	18.9	6.2	41.1

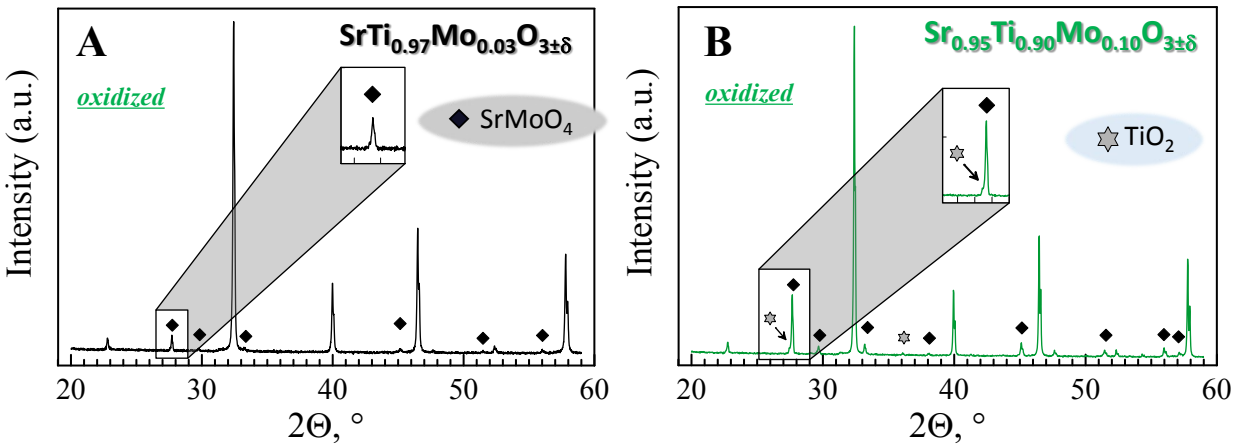

Figure S1. Room-temperature XRD patterns of the oxidized $SrTi_{0.97}Mo_{0.03}O_{3\pm\delta}$ (A) and $Sr_{0.95}Ti_{0.90}Mo_{0.10}O_{3\pm\delta}$ (B).

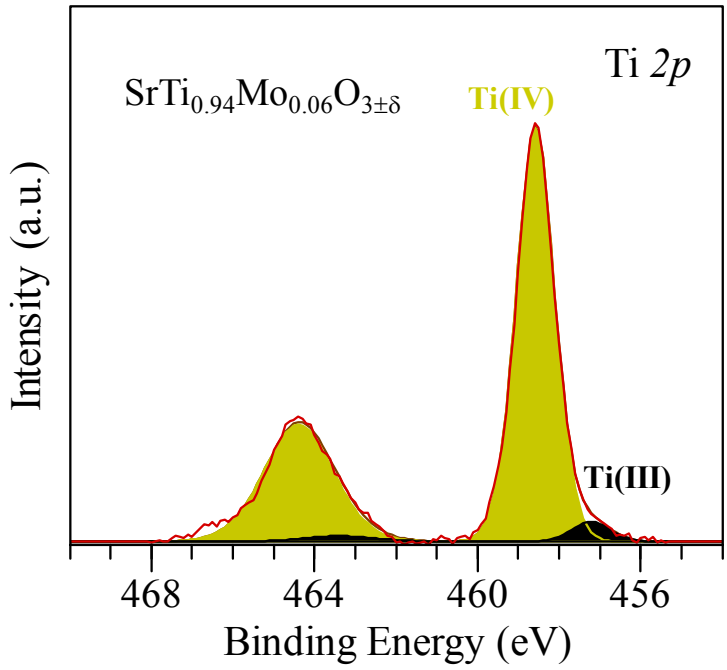

Figure S2. High-resolution XPS spectrum in Ti *2p* region with the corresponding fit for $SrTi_{0.94}Mo_{0.06}O_{3\pm\delta}$ sample.

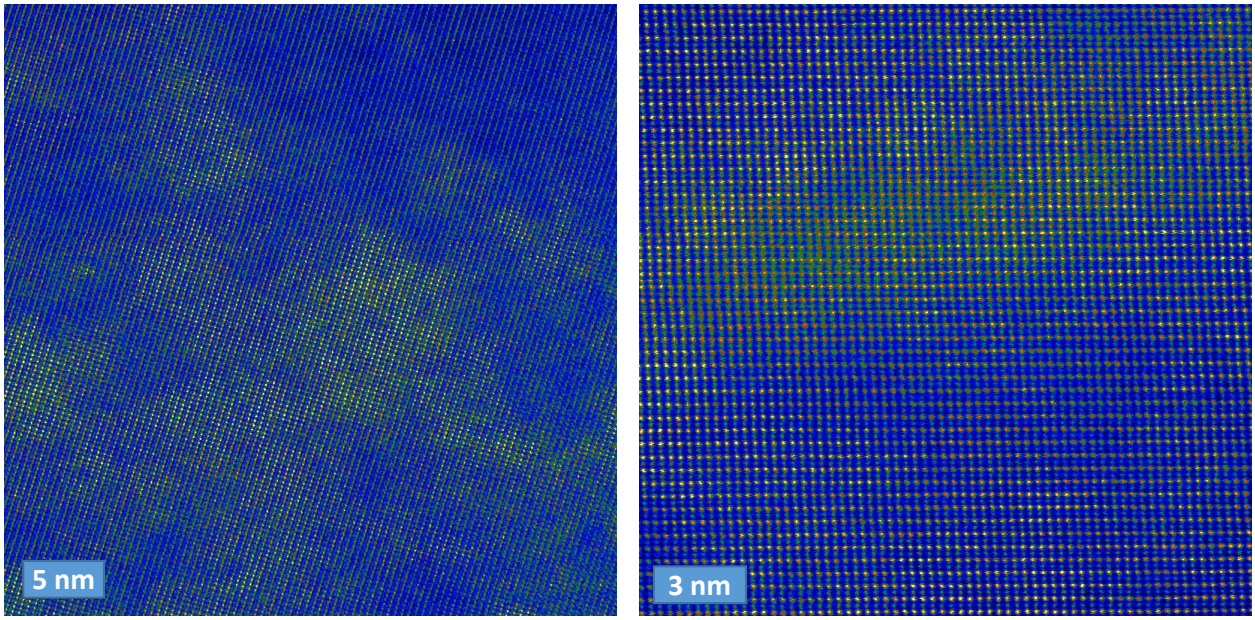

Figure S3. Atomic-resolution elemental maps (blue – lighter, red – heavier) for $Sr_{0.97}Ti_{0.94}Mo_{0.06}O_{3\pm\delta}$ showing nano-islands composed of $SrMoO_3$- inclusions.

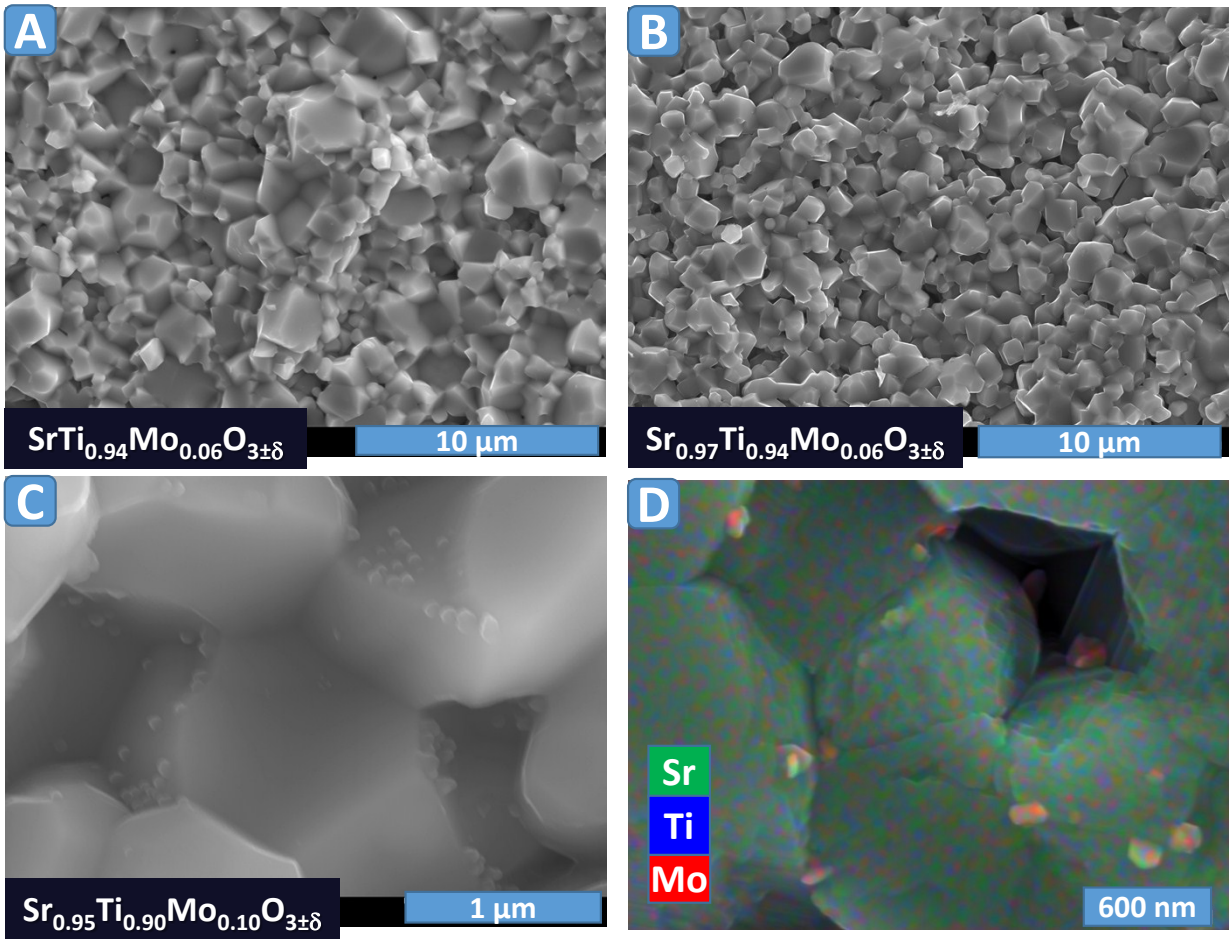

Figure S4. Representative SEM micrographs of $Sr(Ti,Mo)O_{3\pm\delta}$ fractured ceramic samples (A-C) and EDS mapping results for $Sr_{0.95}Ti_{0.90}Mo_{0.10}O_{3\pm\delta}$ (D).

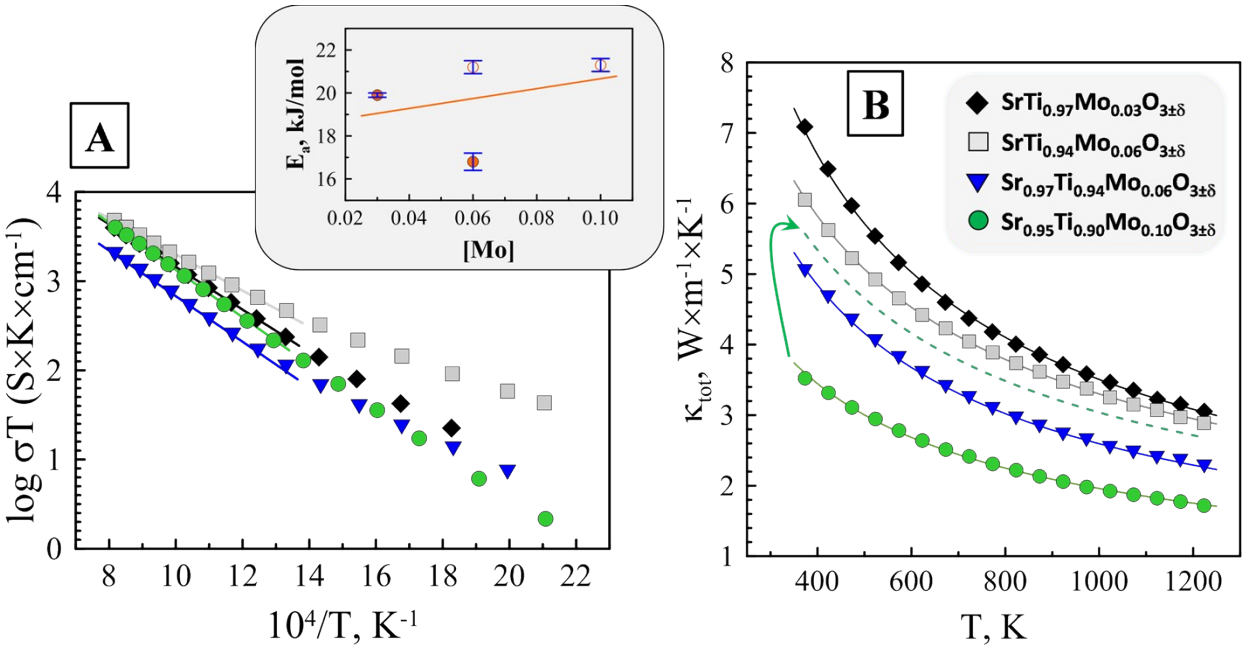

Figure S5. Temperature dependence of the electrical (A) and thermal conductivity (B) of the $Sr(Ti,Mo)O_{3\pm\delta}$ ceramics. The inset in A illustrates the effect of composition on the activation energies of electronic transport at 800-1223 K. The thermal conductivity of $Sr_{0.95}Ti_{0.90}Mo_{0.10}O_{3\pm\delta}$ corrected for porosity effects is shown by a green dashed line.

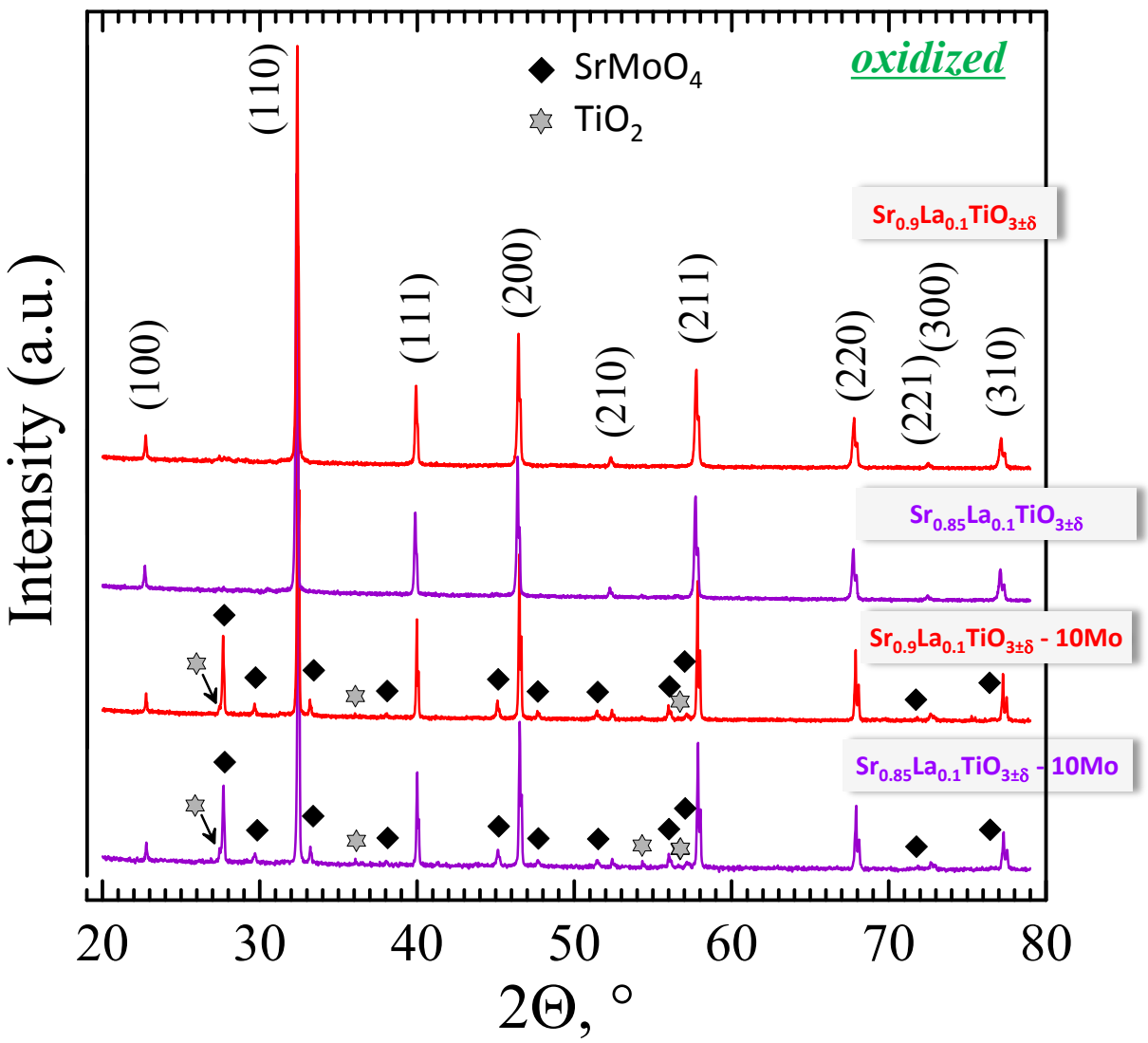

Figure S6. Room-temperature XRD patterns of the oxidized $Sr_{0.9}La_{0.1}TiO_{3\pm\delta}$, $Sr_{0.85}La_{0.1}TiO_{3\pm\delta}$, $Sr_{0.9}La_{0.1}TiO_{3\pm\delta}$ - 10Mo and $Sr_{0.85}La_{0.1}TiO_{3\pm\delta}$ - 10Mo samples.

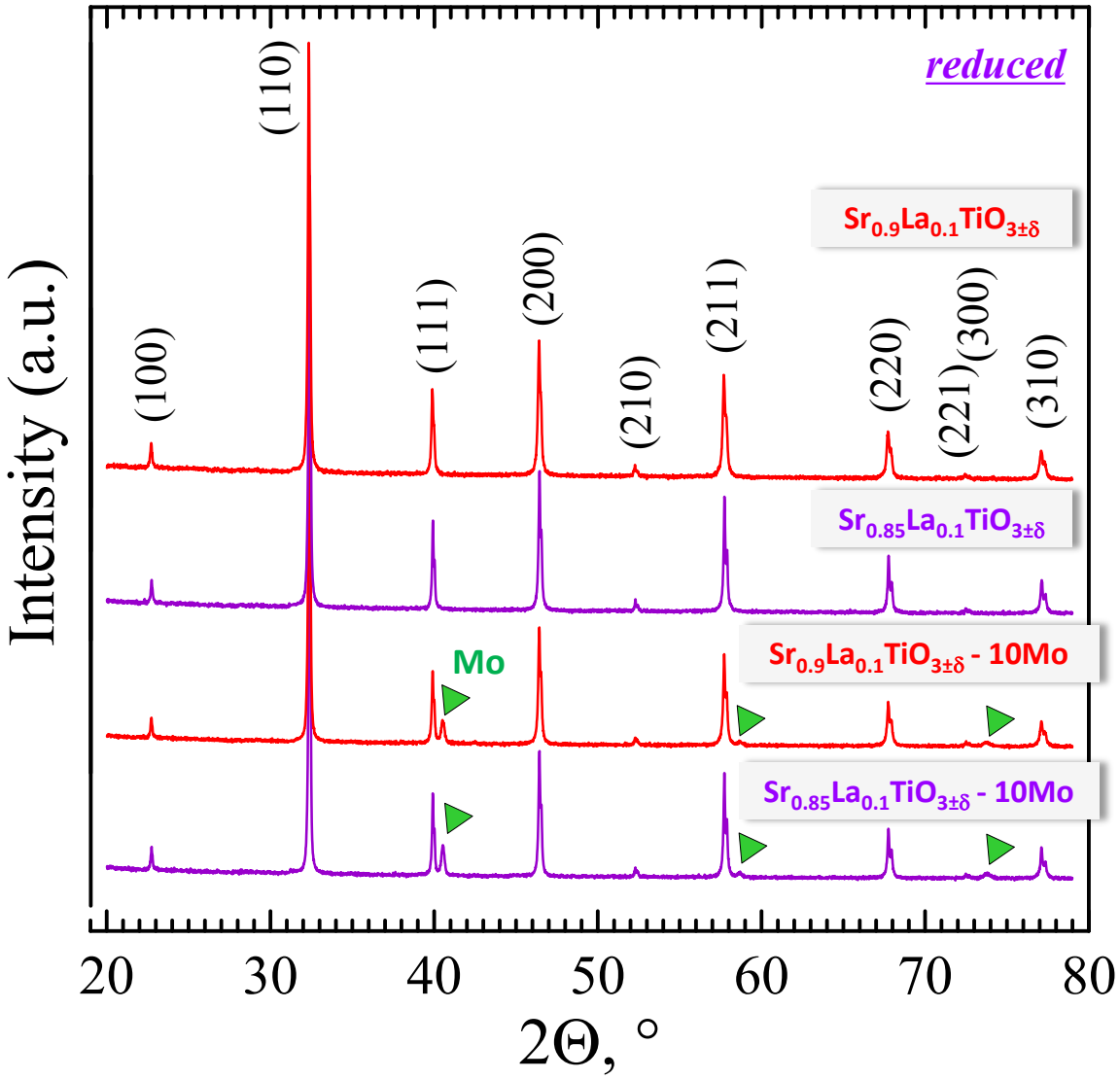

Figure S7. Room-temperature XRD patterns of the reduced $Sr_{0.9}La_{0.1}TiO_{3\pm\delta}$, $Sr_{0.85}La_{0.1}TiO_{3\pm\delta}$, $Sr_{0.9}La_{0.1}TiO_{3\pm\delta}$ - 10Mo and $Sr_{0.85}La_{0.1}TiO_{3\pm\delta}$ - 10Mo samples.

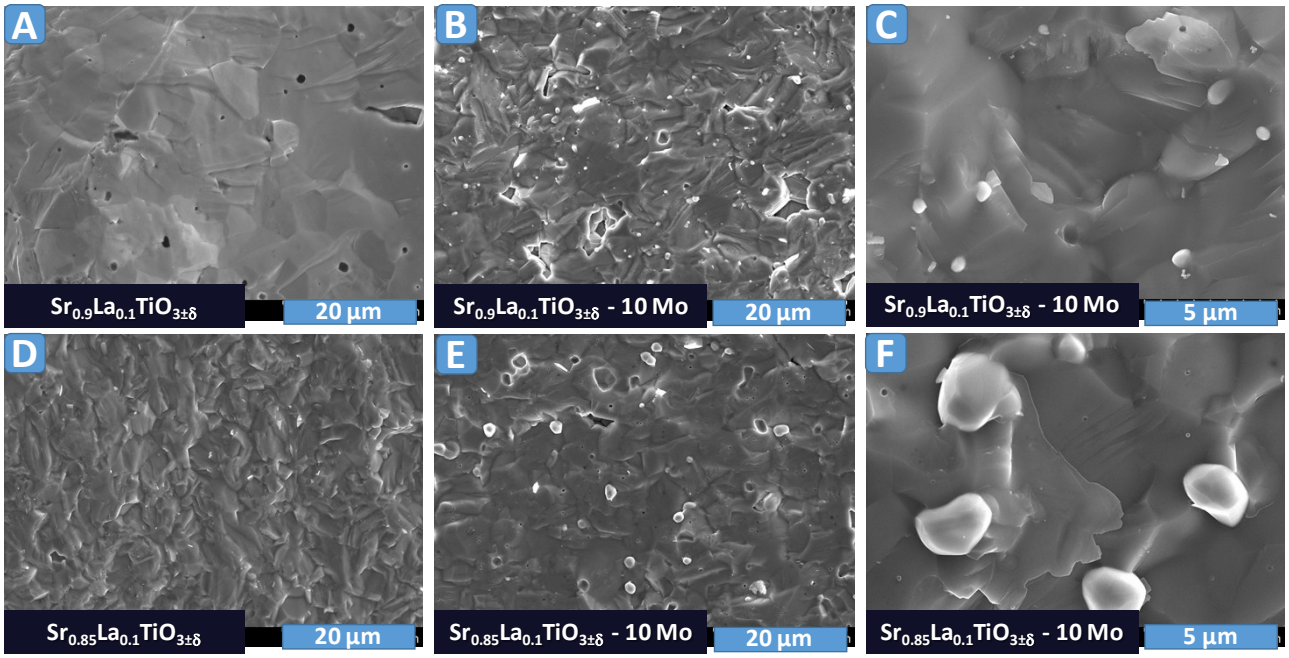

Figure S8. Representative SEM micrographs of the reduced fractured $Sr_{0.9}La_{0.1}TiO_{3\pm\delta}$ (A), $Sr_{0.9}La_{0.1}TiO_{3\pm\delta}$ - 10Mo (B,C), $Sr_{0.85}La_{0.1}TiO_{3\pm\delta}$ (D) and $Sr_{0.85}La_{0.1}TiO_{3\pm\delta}$ - 10Mo (E,F) samples.

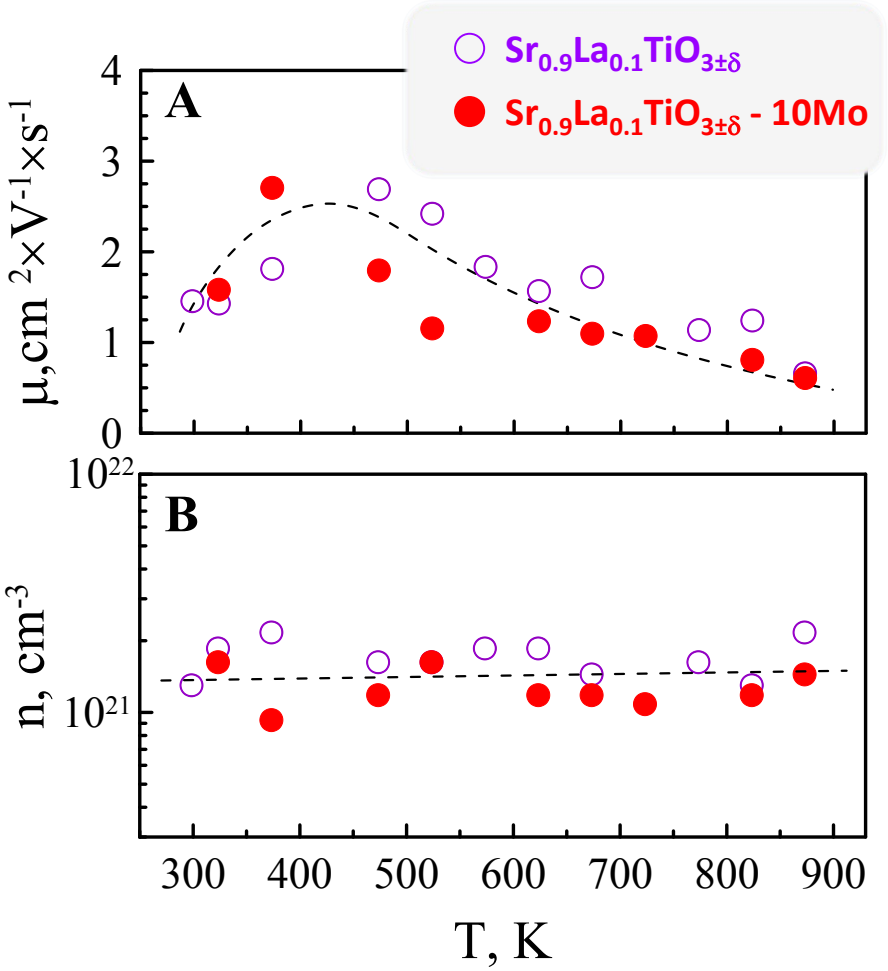

Figure S9. Temperature dependence of the measured charge carrier mobility (A) and charge carrier concentration (B) for reduced $Sr_{0.9}La_{0.1}TiO_{3\pm\delta}$ and $Sr_{0.9}La_{0.1}TiO_{3\pm\delta}$ - 10Mo ceramic samples.